DOI: 10.1002/asia.200700363

Self-Assembly of [*B*-SbW_9O_{33}]$^{9-}$ Subunit with Transition Metal Ions (Mn^{2+}, Cu^{2+}, Co^{2+}) in Aqueous Solution: Syntheses, Structures and Magnetic Properties of Sandwich Type Polyoxometalates with Subvalent Sb^{III} Heteroatom

Jing-Ping Wang, Peng-Tao Ma, Jie Li, Hong-Yu Niu, and Jing-Yang Niu*[a]

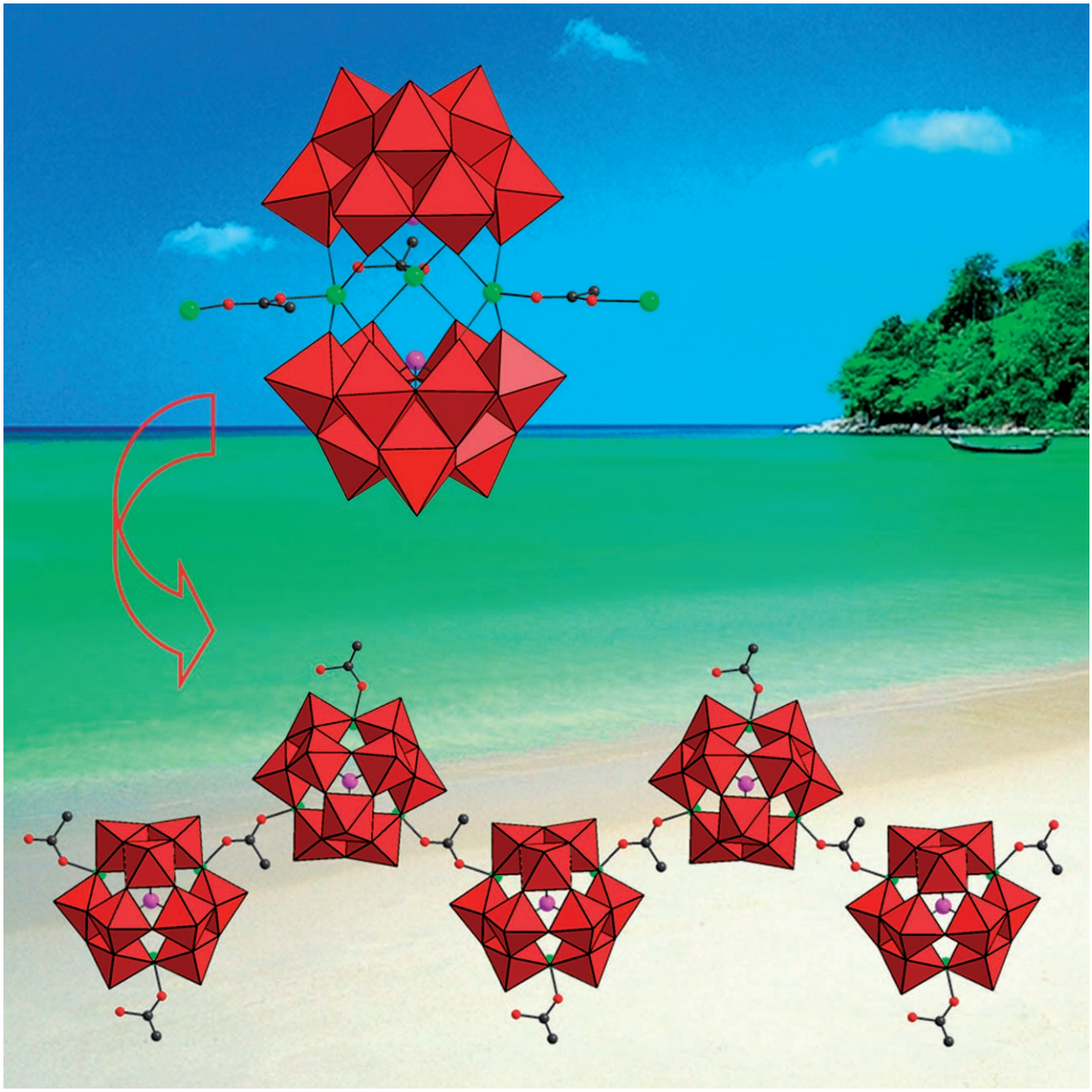

Abstract: Rational self-assembly of Sb_2O_3 and Na_2WO_4, or $(NH_4)_{18}[NaSb_9W_{21}O_{86}]$ with transition-metal ions (Mn^{2+}, Cu^{2+}, Co^{2+}), in aqueous solution under controlled conditions yield a series of sandwich type complexes, namely, $Na_2H_2[Mn_{2.5}W_{1.5}(H_2O)_8(B\text{-}\beta\text{-}SbW_9O_{33})_2]\cdot 32\,H_2O$ **(1)**, $Na_4H_7[Na_3(H_2O)_6Mn_3(\mu\text{-}OAc)_2(B\text{-}\alpha\text{-}SbW_9O_{33})_2]\cdot 20\,H_2O$ (OAc = acetate anion) **(2)**, $NaH_8[Na_2Cu_4Cl(B\text{-}\alpha\text{-}SbW_9O_{33})_2]\cdot 21\,H_2O$ **(3)**, $Na_8K[Na_2K(H_2O)_2\{Co(H_2O)\}_3(B\text{-}\alpha\text{-}SbW_9O_{33})_2]\cdot 10\,H_2O$ **(4)**, and $Na_5H[\{Co(H_2O)_2\}_3W(H_2O)_2(B\text{-}\beta\text{-}SbW_9O_{33})_2]\cdot 11.5\,H_2O$ **(5)**. These structures are determined by using the X-ray diffraction technique and further characterized by obtaining IR spectra and performing elemental analysis. Structure analysis reveals that polyoxoanions in **1** and **5** comprise of two $[B\text{-}\beta\text{-}SbW_9O_{33}]^{9-}$ building units, whereas **2**, **3**, and **4** consist of two isomerous $[B\text{-}\alpha\text{-}SbW_9O_{33}]^{9-}$ building blocks, which are all linked by different transition-metal ions (Mn^{2+}, Cu^{2+}, or Co^{2+}) with different quantitative nuclearity. It should be noted that compound **2** represents the first one-dimensional sinusoidal chain based on sandwich like tungstoantimonate building blocks through the carboxylate-bridging ligands. Additionally, **3** is constructed from sandwiched anions $[Na_2Cu_4Cl(B\text{-}\alpha\text{-}SbW_9O_{33})_2]^{9-}$ linked to each other to form an infinitely extended 2D network, whereas **5** shows an interesting 3D framework built up from offset sandwich type polyoxoanion $[\{Co(H_2O)_2\}_3W(H_2O)_2(B\text{-}\beta\text{-}SbW_9O_{33})_2]^{6-}$ linked by Co^{2+} and Na^+ ions. EPR studies performed at 110 K and room temperature reveal that the metal cations (Mn^{2+}, Cu^{2+}, Co^{2+}) reside in a square-pyramidal geometry in **2**, **3**, and **4**. The magnetic behavior of **1**–**4** suggests the presence of weak antiferromagnetic coupling interactions between magnetic metal centers with the exchange integral $J = -0.552\ cm^{-1}$ in **2**.

Keywords: antimony · polyoxometalates · sandwich complexes · self-assembly · tungsten

Introduction

The current interest in polyoxometalate (POM) chemistry not only stems from their potential applications in analytical science, materials science, catalysis, and medicine, but also from their enormous structural variety and multitude of fascinating properties.[1,2] The design and synthesis of large inorganic high(giant)-nuclear wheels or clusters with multi-dimensional pores,[3,4] or biological modeling[5] have recently constituted an emerging area of interest. Great efforts have been taken toward the decoration of polyoxoanions using organic ligands or transition-metal-complex cations, and the discovery of new structural types with interesting topologies and properties. Meanwhile, it should be pointed out that the formation mechanisms of POMs still remain elusive arising from the many species obtained by the "one-pot" synthesis-commonly described as self-assembly. Therefore, the rational design, synthesis, and characterization of novel POMs with predetermined structures and functions offer an ongoing challenge.

In POM chemistry, transition-metal substituted POMs (TMSPs) are well known, and to date, numerous such complexes have been reported.[6] Among the well-known class of TMSPs, the sandwich type species represent the largest subfamily.[7] The Weakly-,[8] Hervé-,[9] Krebs-,[10] and Knoth-[11]sandwich type polyoxoanions have been obtained to date. However, considering that TMSPs may be of interest for their magnetism as well as their optical, electronic, and catalytic properties,[12–14] the incorporation of paramagnetic transition-metal ions to the centre of sandwich type polyoxoanions remains a focus of POMs. Furthermore, trivacant Keggin type polyoxoanions $[XW_9O_{33or34}]^{n-}$ (X = P, As, Si, Ge, Sb, Bi, Zn) are fundamental building units to construct sandwich type polyoxoanions. The trivacant $\{SbW_9\}$ unit is denoted as the *B*-type fragment derived from a Keggin polyoxoanion. In this case, three edge-shared WO_6 octahedra are removed because the central Sb^{III} heteroatom owns a lone pair of electrons.[15] Moreover, the *B*-type fragment contains two isomers (α and β), which can be derived from the α-Keggin and the β-Keggin framework, respectively. This trivacant building block can be used for synthesis of sandwich like complexes, for example, $[(VO)_3(SbW_9O_{33})_2]^{12-}$ in which two $B\text{-}\alpha\text{-}[SbW_9O_{33}]^{9-}$ moieties are linked by a belt of three VO^{2+} ions.[16]

The class of Sb^{III}-containing polyoxotungstates has been known for a long time.[17] The presence of a lone pair of electrons on the heteroatom precludes the closing of the Keggin unit, allowing many novel POMs with unprecedented structure to be obtained. The first structurally character-

[a] Prof. J.-P. Wang, P.-T. Ma, J. Li, H.-Y. Niu, Prof. J.-Y. Niu
Institute of Molecular and Crystal Engineering
School of Chemistry and Chemical Engineering
Henan University
Kaifeng, Henan, 475004 (P.R. China)
Fax: (+86) 378-388-6876
E-mail: jyniu@henu.edu.cn

Supporting information for this article is available on the WWW under http://www.chemasianj.org or from the author.

ized tungstoantimonate $[NaSb_9W_{21}O_{86}]^{18-}$ displays a large cryptand structure,[17] and subsequently, Wang and co-workers reported the extended 1D structural compound $(NH_4)_{15}Co_{0.5}(NH_3)_3[Co(NH_3)_4NaSb_9W_{21}O_{86}]\cdot 15H_2O$.[18] In the past decades, Yamase and co-workers described the formation and structure of $K_{18.5}H_{1.5}[Ce_3(CO_3)(SbW_9O_{33})(W_5O_{18})]\cdot 14H_2O$ and $[Eu_3(H_2O)_3(SbW_9O_{33})(W_5O_{18})_3]^{18-}$,[19] which are all based on α-$[SbW_9O_{33}]^{9-}$ and $[W_5O_{18}]^{6-}$ groups. Recently, their group reported another two lanthanide-polyoxotungstates, $[(W_5O_{18})Ln(\alpha\text{-}SbW_9O_{33})Ln(H_2O)_2(W_5O_{18})_3]^{15-}$ (Ln = Eu, Dy, Er) and $[Lu_3(H_2O)_4(SbW_9O_{33})_2(W_5O_{18})_2]^{21-}$.[20] In addition, they described the synthesis, structure, heat capacity, and magnetization of $[(VO)_3(SbW_9O_{33})_2]^{12-}$.[16,21] In recent years, the group of Krebs reported the systematic syntheses of large Sb^{III} containing heteropolyanions $[SbW_9O_{33}]^{9-}$, $[Na_2Sb_8W_{36}O_{132}(H_2O)_4]^{22-}$, $[Sb_2W_{22}O_{74}(OH)_2]^{12-}$, $[Sb_2W_{20}M_2O_{70}(H_2O)_6]^{[14-2n]-}$ ($M^{n+}=Fe^{3+}$, Co^{2+}, Mn^{2+}, Ni^{2+}), $[(Mn(H_2O))_3(SbW_9O_{33})_2]^{12-}$, $(C_{52}H_{60}NO_{12})_{12}[(Mn(H_2O))_3(SbW_9O_{33})_2]$, $[M_2(H_2O)_6(WO_2)_2(SbW_9O_{33})_2]^{10-}$ ($M=Zn^{II}$, Mn^{II}), $(NH_4)_{10}[Sb_2W_{20}Co_2O_{70}(H_2O)_6]\cdot 13H_2O$, and $K_6NaH[Sb_2W_{20}Fe_2O_{70}(H_2O)_6]\cdot 13H_2O$,[22] which were all synthesized from the [*B*-α-$SbW_9O_{33}]^{9-}$ fragment. The manganese(II)-substituted polyoxometalate $[(Mn(H_2O))_3(SbW_9O_{33})_2]^{12-}$ has been shown to be a highly efficient catalytic activator in the epoxidation of alkenes.[22b] Subsequently, Kortz et al. reported $[(\alpha\text{-}SbW_9O_{33})_2M_3(H_2O)_3]^{12-}$ ($M=Cu^{2+}$, Zn^{2+}), $K_{12}[Sb_2W_{18}\{Cu(H_2O)\}_3O_{66}]$, $[Fe_4(H_2O)_{10}(\beta\text{-}SbW_9O_{33})_2]^{6-}$, $[Cs_2Na(H_2O)_{10}Pd_3(\alpha\text{-}Sb^{III}W_9O_{33})_2]^{9-}$,[23] all of which are sandwich type compounds based on two α- or β-type SbW_9O_{33} subunits. Very recently, the groups of Kortz and Proust, reported on $(CsNa_2[\{Sn(CH_3)\}_3(H_2O)_4(\beta\text{-}SbW_9O_{33})]\cdot 7H_2O)_\infty$,[24] and $[Sb_2W_{20}O_{70}\{\rho\text{-cymene}\}_2]^{10-}$,[25] respectively, being the first organotin derivative of β-$[SbW_9O_{33}]^{9-}$, and the first obtained organometallic heteropolytungstate related to $[Sb_2W_{22}O_{74}(OH)_2]^{12-}$ by self-assembly, respectively. Yamase et al. have reported a Mn_6 hexagon sandwiched polyoxometalate $[(MnCl)_6(SbW_9O_{33})_2]^{12-}$ and discussed the ferromagnetic properties of five fold coordination Mn_6^{12+} hexagons.[26]

It can be noted that most of the transition-metal-substituted tungstoantimonates are dimeric and sandwich like compounds. Moreover, most of them are discrete structures. The linking of sandwich type Sb–W–O clusters into extended structures remains largely unexplored. Hence, the exploitation of assembling POMs into 1D, 2D, and even 3D frameworks is still in its infancy. We have successfully prepared some novel 1D, 2D, and 3D extended structures constructed from TMSPs clusters. Herein, we describe the syntheses and structural characterizations of the following five POMs based on sandwich type tungstoantimonates clusters as building units: $Na_2H_2[Mn_{2.5}W_{1.5}(H_2O)_8(B\text{-}\beta\text{-}SbW_9O_{33})_2]\cdot 32H_2O$ **(1)** ≡ Na_2H_2-**1a**·$32H_2O$, $Na_4H_7[Na_3(H_2O)_6Mn_3(\mu\text{-}OAc)_2(B\text{-}\alpha\text{-}SbW_9O_{33})_2]\cdot 20H_2O$ **(2)** ≡ Na_4H_7-**2a**·$20H_2O$ (OAc = acetate anion, CH_3COO^-), $NaH_8[Na_2Cu_4Cl(B\text{-}\alpha\text{-}SbW_9O_{33})_2]\cdot 21H_2O$ **(3)** ≡ NaH_8-**3a**·$21H_2O$, $Na_8K[Na_2K(H_2O)_2\{Co(H_2O)\}_3(B\text{-}\alpha\text{-}SbW_9O_{33})_2]\cdot 10H_2O$ **(4)** ≡ Na_8K-**4a**·$10H_2O$, $Na_5H[\{Co(H_2O)_2\}_3W(H_2O)_2(B\text{-}\beta\text{-}SbW_9O_{33})_2]\cdot 11.5H_2O$ **(5)** ≡ Na_5H-**5a**·$11.5H_2O$. The solid-state structure of **2** is the first example of a one-dimensional sinusoidal chain based on sandwich type polyoxoanion **2a** bridged by an organic carboxylate ligand. **3a** polyoxoanions connect to each other to build a 2D network, a phenomenon reported for the first time in antimony-containing sandwich POMs chemistry. More interestingly, compound **5** is a sandwich type complex with three cobalt atoms and a tungsten atom incorporated into the belt of the polyoxoanion, which is linked with an adjacent same framework, generating a 3D network, by the linkage of cobalt and sodium atoms. To the best of our knowledge, the example of 3D infinitely netlike structures constructed from sandwich type tungstoantimonate anions has rarely been reported.

Abstract in Chinese:

以Sb_2O_3和Na_2WO_4或$(NH_4)_{18}[NaSb_9W_{21}O_{86}]$为原料与过渡金属离子($Mn^{2+}$, Cu^{2+}, Co^{2+})在水溶液中反应，通过控制反应条件制备了 5 种夹心结构锑钨酸盐。其中化合物 1 和 5 包含两个[B-β-$SbW_9O_{33}]^{9-}$建筑单元，而 2，3，4 由两个异构的[*B*-α-$SbW_9O_{33}]^{9-}$建筑块通过不同数量的过渡金属离子相连而成。化合物 1 是首例通过草酸根桥连而成的一维正弦链状结构夹心锑钨酸盐；化合物 3 基于四核铜取代的三明治型单元$[Na_2Cu_4Cl(B\text{-}\alpha\text{-}SbW_9O_{33})_2]^{9-}$通过Cu-O-W桥连形成 2D结构；化合物5包含错位的夹心多阴离子$[\{Co(H_2O)_2\}_3W(H_2O)_2(B\text{-}\beta\text{-}SbW_9O_{33})_2]^{6-}$并展示出 3D网状结构框架。EPR研究表明，化合物 2，3，4 中Mn^{2+}, Cu^{2+}, Co^{2+}离子都处于四方锥构型。磁性研究显示，化合物 1–4 的磁性核之间存在弱的反铁磁耦合作用。

Results and Discussion

Synthesis

Based on previous work, we further explored the synthetic strategy of sandwich type tungstoantimonates. In our experiment, we do not use the common [*B*-$SbW_9O_{33}]^{9-}$ lacunary precursor, but directly employ some raw materials of Sb_2O_3, Na_2WO_4, and transition-metal ions (such as Mn^{2+}). By heating the solution above 80 °C in sodium acetate buffer, we obtain the dominating product of trimanganese-substituted polyoxoanion **2** and the by-product of dimanganese-substituted species **1**. Intriguingly, the synthesis of **2** is accomplished by reaction of the component of acetate buffer with the transition metal Mn^{2+}. In contrast to **1** and **2**, the synthetic strategy of **3**–**5** was developed. Compounds **3**–**5** were all synthesized from a cryptate $[NaSb_9W_{21}O_{86}]^{18-}$ precursor. However, the sandwich type polyoxoanions presented in **3**–**5** contain the [*B*-$SbW_9O_{33}]^{9-}$ building blocks, indicating that during the course of the reaction, the following transformation must have taken place: $[NaSb_9W_{21}O_{86}]^{18-}\rightarrow[B\text{-}SbW_9O_{33}]^{9-}$. **3** was obtained by directly heating the mixture of $[NaSb_9W_{21}O_{86}]^{18-}$ and Cu^{2+} above 80 °C. Whilst the synthetic conditions of **4** and **5** were similar to **3**, the addition of KOH solution (see Experimental Section) is required in the latter. Surprisingly, compounds **4** and **5** were synchronously obtained in one system, which crystallize in the orthorhombic and triclinic systems, respectively. It should be

CHEMISTRY
AN ASIAN JOURNAL

noted that the $[B\text{-}\alpha\text{-}SbW_9O_{33}]^{9-}$ fragment in **4** and $[B\text{-}\beta\text{-}SbW_9O_{33}]^{9-}$ fragment in **5** are the two isomers of the $[B\text{-}SbW_9O_{33}]^{9-}$ polyanion, which indicates the presence of the isomerization equilibrium in the disassembly and reassembly procedure of the cryptate polyoxoanion precursor. During the course of our investigation of these transition-metal-substituted sandwich type tungstoantimonates, we discovered that control of reaction conditions is more important than precursor type. From the analyses on the synthetic conditions mentioned previously, we can see that many factors (temperature and time of heating, pH value, ionic strength, concentration of reaction system) can influence the type of building blocks, the amount of transition metal incorporating into the core of sandwich type complexes, and the extended structural fashion. Hence, further investigation on this work is in progress.

Description of the Crystal Structures

The structures of compounds **1**–**5** were determined by using the single-crystal X-ray diffraction technique and characterized by elemental analysis and FTIR spectroscopy. The selected bond lengths are listed in Table S1 in the Supporting Information.

The polyoxoanion of **1a** is isomorphous to, but different from the previously reported $[Sb_2W_{20}M_2O_{70}(H_2O)_6]^{[14-2n]-}$,[22a] mainly arsing from the site occupancy disorder of two W10 atoms (each of the two opposite W10 sites is occupied by a W atom and an Mn atom with the site occupancy factor of 75% and 25%, respectively). The bond valence of all the Mn and W atoms in **1** are +2 and +6, respectively, which were validated by the XPS results (see Figure S1 and S2 in the Supporting Information). As a result, the polyoxoanion framework of **1a** with idealized C_{2v} point symmetry is constructed from two trivacant $[B\text{-}\beta\text{-}SbW_9O_{33}]^{9-}$ subunits linked by 2.5 octahedral Mn^{II} and 1.5 octahedral W^{VI} ions leading to a sandwich type structure (Figure 1). All Mn^{2+} centers are octahedrally coordinated, defined by three oxygen atoms from two $[B\text{-}\beta\text{-}SbW_9O_{33}]^{9-}$ moieties and other oxygen atoms from water molecules. The W10 atom is also octahedrally coordinated by four oxygen atoms from two $[B\text{-}\beta\text{-}SbW_9O_{33}]^{9-}$ fragments and two water ligands. The bond lengths of Mn–O vary from 2.115(8) to 2.217(9) Å, whereas the angles are in the range of 82.6(3)–96.9(4)°, which are all in the common ranges. The four metal atoms lie at the corners of a rhombus with the adjacent two edges of 10.186 and 5.980 Å. Additionally, the formation of infinite chain structure is formed of adjacent cluster anions of **1** alternating with bridging $[Na_2(H_2O)_4]^+$ groups.

To our knowledge, compound **2** represents the first one-dimensional sinusoidal chain based on sandwich like tungstoantimonate building blocks through the carboxylate-bridging ligands (Figure 2c and Figure S3 in the Supporting Information). Although **2** was obtained in the same system as **1**, it was clearly different in the structural construction. The polyoxoanion **2a** with the D_{3h} point symmetry is composed of two $[B\text{-}\alpha\text{-}SbW_9O_{33}]^{9-}$ fragments combined together

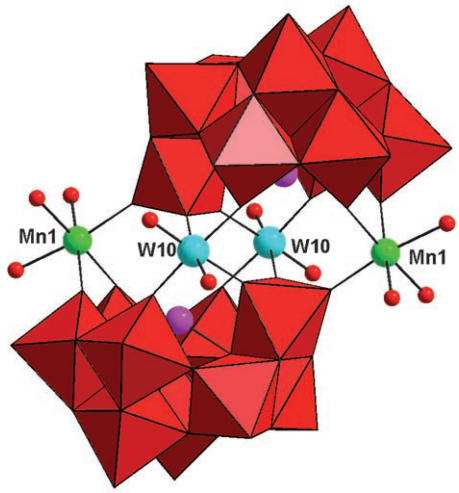

Figure 1. Polyhedral and ball-and-stick representation of the polyoxoanion **1a** with the molecular formula $[Mn_{2.5}W_{1.5}(H_2O)_8(B\text{-}\beta\text{-}SbW_9O_{33})_2]^{4-}$. The WO_6 octahedra are shown in red, and the balls represent Sb (purple), Mn/W (cyan), Mn (green), O (red). The hydrogen atoms are omitted for clarity.

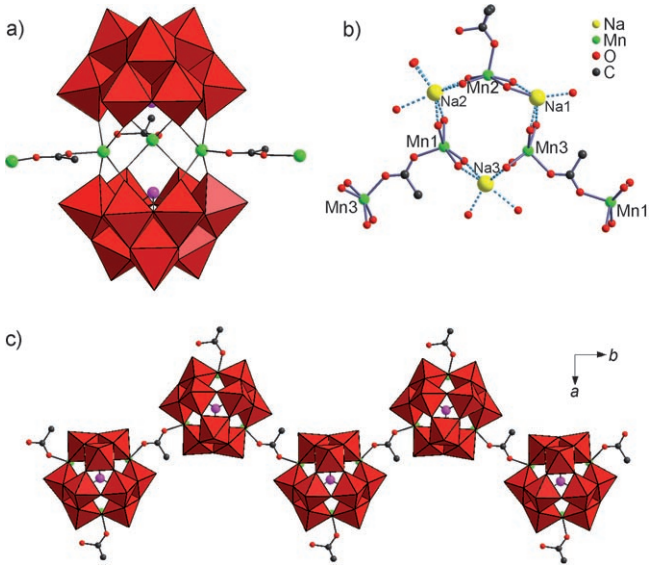

Figure 2. a) Combined polyhedral/ball-and-stick representation of $[Na_3(H_2O)_6Mn_3(m\text{-}OAc)_2(B\text{-}\alpha\text{-}SbW_9O_{33})_2]^{11-}$ (**2a**), the sodium counterions are omitted for clarity. b) Ball-and-stick representation of the connection mode in central belt of **2a**. c) Polyhedral/ball-and-stick representation of the structure of compound **2** down the *c*-axis. The WO_6 octahedra are shown in red, and the balls represent Sb (purple), Na (yellow), Mn (green), W (cyan), C (black), and O (red). The hydrogen atoms are omitted for clarity.

by three $[Mn(OAc)]^+$ groups and three Na^+ ions in an alternating mode, resulting in the sandwich type structure (Figures 2a and b). The structure is closely related to the previously reported trinuclear manganese(II)-substituted tungstoantimonate $[(Mn(H_2O))_3(SbW_9O_{33})_2]^{12-}$.[22b] A striking difference between them is that the acetate ligand replacing a water molecule participates in the coordination to manganese cations. Each Mn^{2+} ion resides in the square pyramidal

coordination geometry with the mean Mn–O distance of 2.086 Å (Table S1 of the Supporting Information). It is worth noting that every manganese ion coordinates to an acetate ligand rather than a terminal water molecule in the central sandwich layer. Moreover, the acetate ligands employ two types of coordination patterns in the structural construction: one is only coordinating to a manganese atom (Mn2) by a carboxylate oxygen atom, and the other is by acting as a bidentate ligand in simultaneous connection with two manganese atoms (Mn1 and Mn3) from different polyoxoanion framework (see Figures 2a and b). By means of this construction motif, adjacent cluster anions **2a** are able to construct an unprecedented one-dimensional sinusoidal chain by the acetate bridges. In addition, the C2 atom in the methyl group of the acetate ligand coordinating to the Mn2 atom is disordered with 50% probability over two positions (Figure 2b).

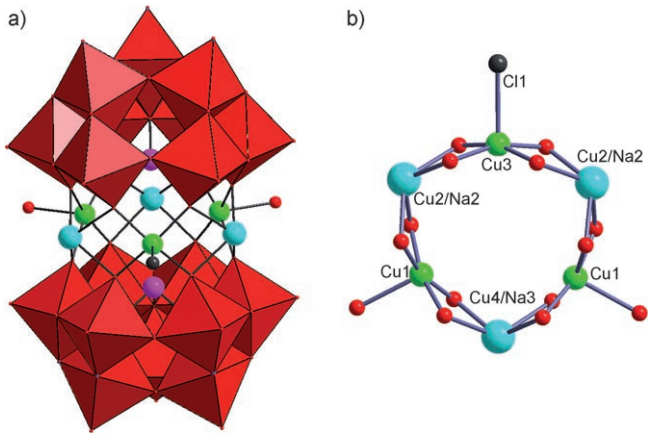

Figure 3. a) Combined polyhedral/ball-and-stick representation of $[Na_2Cu_4Cl(B\text{-}\alpha\text{-}SbW_9O_{33})_2]^{9-}$ (**3a**). b) Ball-and-stick representation of the central belt in **3a**. The WO_6 octahedra are shown in red, and the balls represent Cu (green), Sb (purple), Cu/Na (cyan), Cl (black), and O (red).

Figure 3a depicts the structure of polyoxoanion **3a**. The anion consists of a $\{Cu_4Na_2\}$ hexagon moiety sandwiched by two $[B\text{-}\alpha\text{-}SbW_9O_{33}]^{9-}$ building blocks, which exhibits a sandwich type structure framework similar to recently reported $[(CuCl)_6(AsW_9O_{33})_2]^{12-}$ and $[(MnCl)_6(SbW_9O_{33})_2]^{12-}$.[26] The $\{Cu_4Na_2\}$ hexagon moiety contains three square pyramidal isolated Cu^{2+} ions and three disordered four-coordinate Cu^{2+} ions as shown in Figure 3b, each of which is coordinated by two $[B\text{-}\alpha\text{-}SbW_9O_{33}]^{9-}$ fragments. The square-pyramidal-coordinated Cu^{2+} centers can be grouped as two different types: the two identical CuO_5 and a CuO_4Cl group, which are all coordinated by four interior oxygen atoms from two $[B\text{-}\alpha\text{-}SbW_9O_{33}]^{9-}$ ligands with the vertex position occupied by O (for Cu1) or Cl (for Cu3) atoms (see Figures 3a and b). The three five-coordinate Cu^{2+} ions were arranged in an approximately equilateral triangle with Cu1···Cu1 = 4.896(3) Å, Cu1···Cu3 = 4.904(4) Å, and Cu···Cu···Cu = 60°. The Cu–O bond distances are in the range of 1.928(13)–2.323(16) Å for Cu1 atoms, and 1.920(14) Å for Cu3 atom with the Cu3–Cl length of 2.605(13) Å. (Table S1 in the Supporting Information) The Cu2 and the Cu4 centers show highly disordered positions, which are the preferential positions on the Na2 (60%) and Na3 (80%) sites, respectively. Moreover, the three positions occupied by disordered copper atoms were arranged in a bigger triangle, which were just bound by two $[B\text{-}\alpha\text{-}SbW_9O_{33}]^{9-}$ ligands with the average bond lengths of 2.217 and 2.262 Å for Cu2–O and Cu4–O, respectively (see Table S1 in the Supporting Information). The XPS spectra reveal the bond valences of all the Cu and W atoms in **3** as +2 and +6, respectively (Figure S4 and S5 in the Supporting Information).

The solid-state structure of **3** reveals a beautiful 2D network as shown in Figure 4, which can be thought of as the structure of a tetra-copper-substituted cluster anion $[Cu_4K_2(H_2O)_8(\alpha\text{-}AsW_9O_{33})_2]^{8-}$.[29] Each polyoxoanion **3a** is connected to four neighbours by four Cu1–O4–W4 bridges, leading to a 2D network. (see Figure 4 and Figure S6 in the Supporting Information) The two equivalent copper centers (Cu1) in the belt region of **3a** are linked to the tungsten atoms (W4) in the "cap" sites from two neighbours through the terminal oxygen atoms. Meanwhile, each of two symmetrically equivalent tungsten centers (W4) in the two "cap" sites is covalently linked to the copper atoms (Cu1) from two adjacent polyoxoanions. In addition, compound **3** can be described as double layers of **3a**, with the Cu–Cl bond of the central belt pointing at each other. Figure 4 shows the solid-state arrangement of polyoxoanion **3a**, which were arrayed alternatingly vertical and horizontal. Each polyoxoanion arranged vertically is completely offset with four peripheral polyoxoanions distributed in the horizontal layer. Aris-

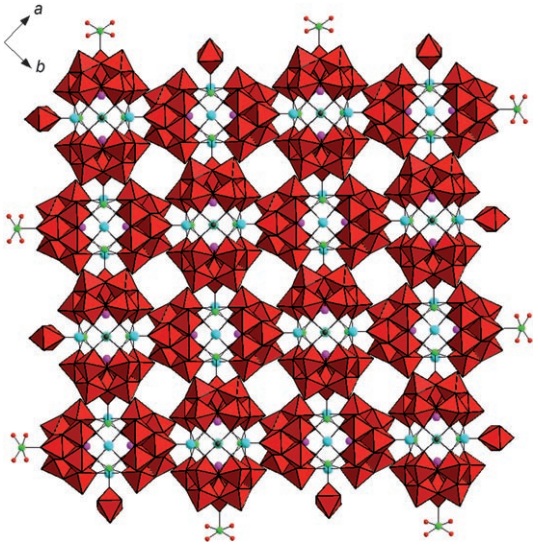

Figure 4. Combined polyhedral/ball-and-stick representation of the two-dimensional arrangement of **3**. The WO_6 octahedra are shown in red, and the balls represent Cu (green), Sb (purple), Cu/Na (cyan), Cl (black), and O (red).

ing from the dint in this construction motif, adjacent cluster anions **3a** are able to construct an attractive 2D network with the Cu–O4–W bridges (Figure 4). To the best of our knowledge, the extended 2D-netlike-structure framework based on sandwich type tungstoantimonate is reported for the first time.

Polyoxoanion **4a** is a dimer of two $[B\text{-}\alpha\text{-}SbW_9O_{33}]^{9-}$ subunits linked by three Co^{2+}, two sodium, and a potassium ion (see Figure 5a and b). The arrangement of nearly hexagonal

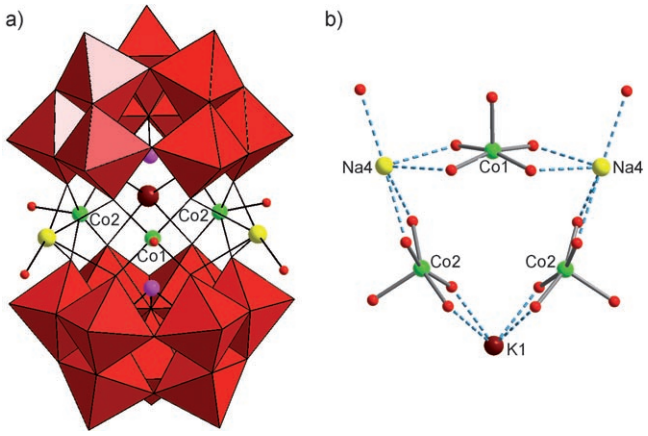

Figure 5. a) Polyhedral and ball-and-stick representation of $[Na_2K(H_2O)_2\{Co(H_2O)\}_3(B\text{-}\alpha\text{-}SbW_9O_{33})_2]^{7-}$ (**4a**). b) Ball-and-stick representation of the central belt in **4a**. The clusters of **4a** are shown in red; and the balls represent Co (green), Sb (purple), W (light blue), Na (yellow), K (carmine), and O (red).

$\{Co_3Na_2K\}$ distribution in the belt region is sandwiched by two $[B\text{-}\alpha\text{-}SbW_9O_{33}]^{9-}$ moieties resulting in the idealized C_{2h} point symmetry. All cobalt ions have a five-coordinate square-pyramidal geometry with the bond distances of Co–O in the range of 1.984(15)–2.096(17) Å (Table S1 in the Supporting Information). The bottom plane is defined by four O atoms from two $[B\text{-}\alpha\text{-}SbW_9O_{33}]^{9-}$ moieties and the axial position is occupied by a terminal water molecule. Each of the two sodium ions in the belt region of **4a** interact with five oxygen atoms, whereas the potassium ion is only chelated by two $[B\text{-}\alpha\text{-}SbW_9O_{33}]^{9-}$ ligands with an average bond length of 2.786 Å. The structure of **4a** is closely related to the recently reported tripalladium-substituted tungstoantimonate(III) $[Cs_2Na(H_2O)_{10}Pd_3(\alpha\text{-}SbW_9O_{33})_2]^{9-}$.[23d] The prominent differences are: a) the palladium(II) ions have a square-planar coordination geometry, and b) the Cs/Na mix-alkaline metal cations are replaced by K^+/Na^+ ions. Moreover, the polyoxoanion **4a** is markedly different to the isostructural tricobalt-substituted tungstosilicate species $[K_2\{Co(H_2O)_2\}_3(SiW_9O_{34})_2]^{12-}$ isolated as a potassium salt.[30] In the polyoxoanion $[K_2\{Co(H_2O)_2\}_3(SiW_9O_{34})_2]^{12-}$, each cobalt ion is bound to two $[SiW_9O_{34}]^{10-}$ moieties by four terminal oxygen atoms and two terminal water molecules, resulting in an octahedral coordination geometry. Nevertheless, the three Co^{2+} ions incorporated into the central belt of the **4a** framework all have square-pyramidal configurations, in such a way that the relevant Co–Co distances range from 5.057(1) to 5.128(2) Å in the triangular $\{Co_3O_{15}\}$ entity.

Compound **5** is of special interest as it contains an offset sandwich type polyoxoanion with two different metals incorporated simultaneously, and is obtained together with **4** in the same system. However, it was clearly different from the structural construction of **4a**, that consists of two $[B\text{-}\beta\text{-}SbW_9O_{33}]^{9-}$ subunits joined together by two Co^{2+} and two disordered Co^{2+}/W^{6+} ions into an assembly with a virtual C_{2v} point symmetry (Figure 6). The central belt of **5a** con-

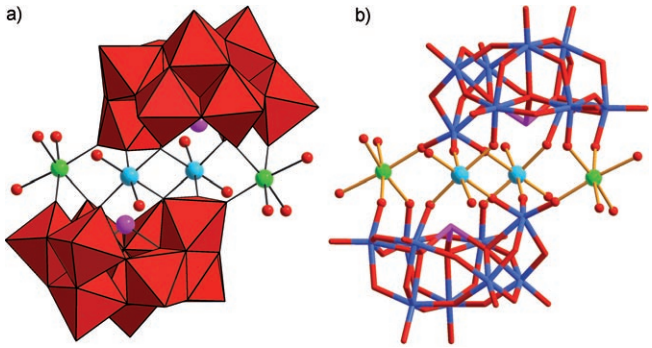

Figure 6. Polyhedral (left) and ball-and-stick (right) representations of $[\{Co(H_2O)_2\}_3W(H_2O)_2(B\text{-}\beta\text{-}SbW_9O_{33})_2]^{6-}$ (**5a**). The clusters of **5a** is shown in red; and the balls represent Co (green), Sb (purple), Co/W (cyan), and O (red).

tains a rhomblike $\{Co_3W\}$ group sandwiched by two screw symmetric $[B\text{-}\beta\text{-}SbW_9O_{33}]^{9-}$ building blocks, meanwhile, the adjacent Co^{2+} and disordered Co^{2+}/W^{6+} ions are bridged by the five-coordinate sodium ions. The separation of exterior Co···Co (10.131(4) or 10.396(5) Å) is clearly longer than the interior two disordered Co···Co (5.930(2) or 5.828(3) Å). In contrast to those in **4a**, each cobalt atom is octahedrally coordinated (2.031(15)–2.264(16) Å) in **5a**, coordinated by four oxygen atoms from three different $[B\text{-}\beta\text{-}SbW_9O_{33}]^{9-}$ ligands and two terminal water molecules. Nevertheless, the two disordered positions in the belt region of **5a** are defined by four O donors from two $[B\text{-}\beta\text{-}SbW_9O_{33}]^{9-}$ ligands and two terminal water molecules with distances of 1.89(2)–2.113(17) Å, each of which is occupied by a cobalt and a tungsten atom with 50% occupation factor for each. Moreover, the Sb atoms incorporated into the $[B\text{-}\beta\text{-}SbW_9O_{33}]^{9-}$ building units are trigonal-pyramidal in geometry with an average bond length of 1.985 Å, (Table S1 of the Supporting Information) and display a longer separation of 5.772(2) or 5.703(2) Å arising from an offset of two $[B\text{-}\beta\text{-}SbW_9O_{33}]^{9-}$ subunits.

The structure of **5a** is likely to be similar to that of decatungsto tungstoantimonate $(NH_4)_{10}[Sb_2W_{20}Co_2O_{70}(H_2O)_6]\cdot 13H_2O$ described by Krebs and co-workers.[22e] The contrasting differences are: 1) two tungsten atoms in the belt is replaced by a tungsten and a cobalt with disordered distribution, 2) each cobalt atom is bound to two water instead of three water molecules, and 3) the lacunae between

the cobalt and antimony atoms in the belt are occupied by four sodium ions rather than four transition metal atoms. In addition, the solid-state arrangement of **5** deserves special attention, exhibiting a remarkable 3D-extended packing. As shown in the construction motif of **5a** (Figure 7), each $[B\text{-}\beta\text{-}SbW_9O_{33}]^{9-}$ subunit in **5a** is joined together with another two $[B\text{-}\beta\text{-}SbW_9O_{33}]^{9-}$ moieties by two cobalt atoms. In this case, an infinite extended 1D chain was generated by the double W–O–Co–O–W bridges (see Figure 7). In addition to the two Co^{II} linkages, the four Na^+ ions incorporated into the central belt also act as joints, linking the different chainsand generating the 3D-extended network (see Figure 8).

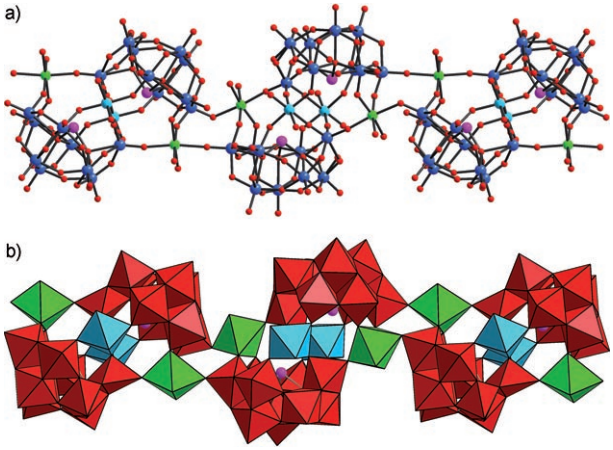

Figure 7. Ball-and-stick representation (top) and polyhedral view (bottom) of the 1D chain in **5**. The WO_6, CoO_6, and disordered MO_6 (M = Co/W) octahedra are shown in red, green, and cyan, respectively, and the balls represent Co (green), Sb (purple), Co/W (cyan), and O (red).

EPR spectra for compound 2–4

The samples studied in this work, which were doped into a slim glass tube, were used in the form of polycrystalline powders. The X-band polycrystalline-powder EPR spectra measured at room temperature and 110 K for **2**, **3**, and **4** were shown in Figure 9, 10, and 11, respectively. As for **2**, the spin Hamiltonian used to represent the EPR spectra of the Mn^{II} ion is given by Equation (1):

$$\hat{H} = g\beta HS + D[S_z^2 - S(S+1)/3] + E(S_x^2 - S_y^2) \qquad (1)$$

where H is the magnetic field vector, g is the spectroscopic splitting factor, β is the Bohr magneton, D is the axial zero field splitting term, E is the rhombic zero field splitting parameter, and S is electron spin vector.[31] If D and E are very small compared to $g\beta HS$, five EPR transitions are expected, $|+5/2> \leftrightarrow |+3/2>$, $|+3/2> \leftrightarrow |+1/2>$, $|+1/2> \leftrightarrow |-1/2>$, $-1/2> \leftrightarrow |-3/2>$ and $|-3/2> \leftrightarrow |-5/2>$. In the X-band polycrystalline-powder EPR spectra of **2** at room temperature (Figure 10), a broad signal is observed with a g value of 2.28, which arises from the dipolar interactions and enhanced-spin-lattice relaxation.[32] The spectrum of **2** at 110 K consists of three resonance absorption bands with effective

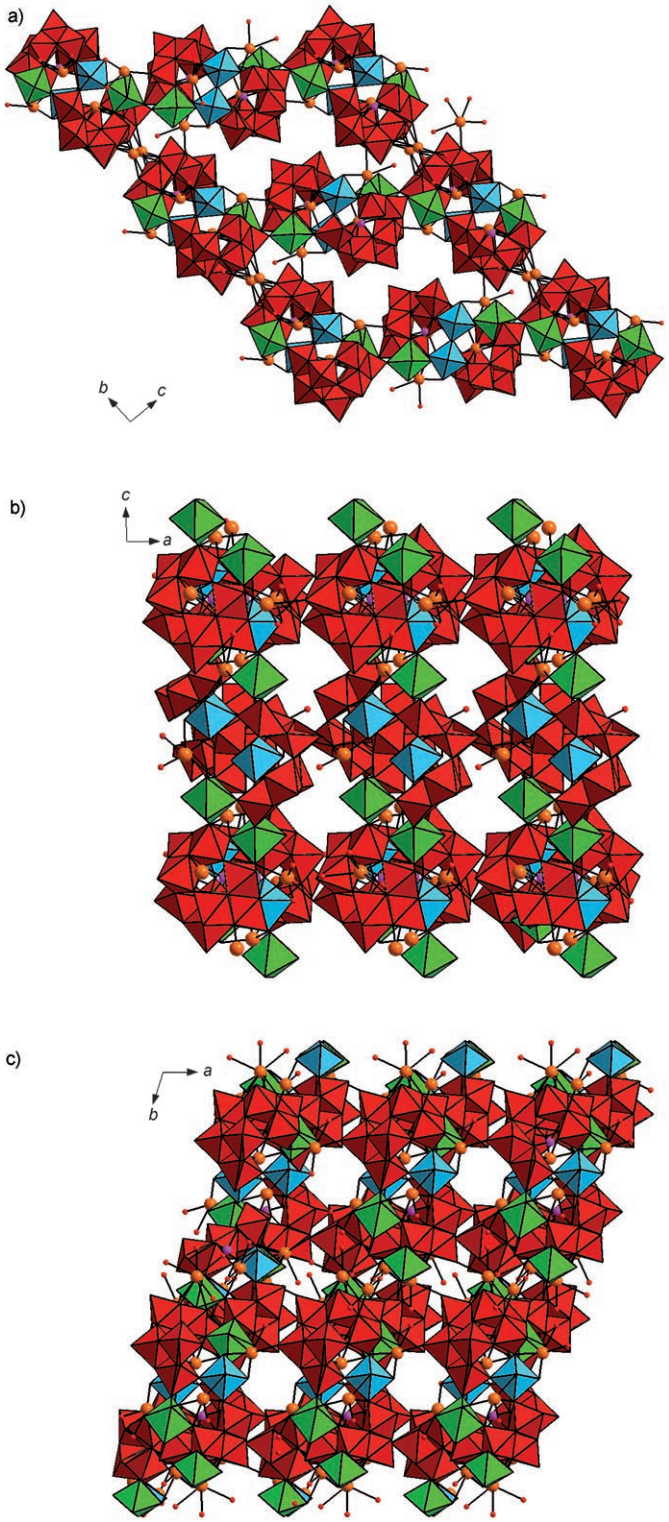

Figure 8. View of the 3D network along a-axis (top), b-axis (middle), and c-axis (bottom) in **5**. The WO_6, CoO_6, and disordered MO_6 (M = Co/W) octahedra are shown in red, green, and cyan, respectively, and the balls represent Co (green), Sb (purple), Co/W (cyan), O (red) and sodium- (orange).

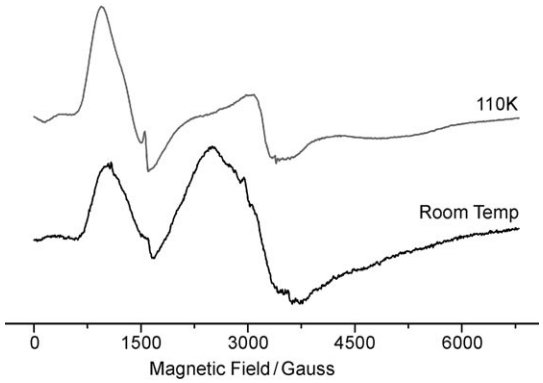

Figure 9. EPR spectra of **2** recorded at 110 and 300 K.

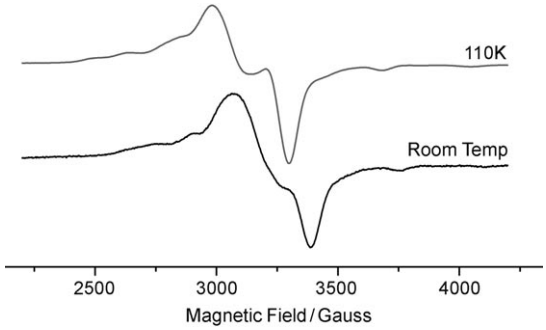

Figure 10. EPR spectra of **3** recorded at 110 and 300 K.

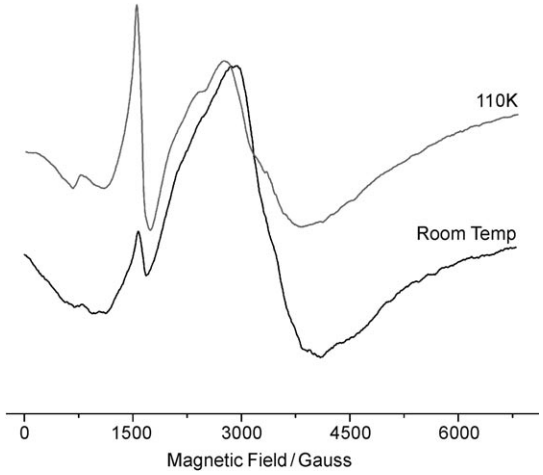

Figure 11. EPR spectra of **4** recorded at 110 and 300 K.

g values of 5.49, 4.29 and 2.09. The resolution is considerably improved compared to the spectra obtained at room temperature, apparently arising from the signal sharpening induced by the increasing spin-lattice relaxation time. Meanwhile, the EPR signals at $g=5.49$ and $g=4.29$ increase whilst the signal at $g=2.09$ decreases. The increase of an isotropic transition around $g=4.29$ arising from an $S=5/2$ trinuclear Mn^{II} system originates from the intermediate Kramers doublet, which is caused by the zero-field splitting effect and the weak spin-orbit coupling.[33]

The room-temperature spectrum for **3** displays an anisotropic broad resonance centered at ca. 3226 G (Figure 10). Moreover, two less intense signals are observed at about 2550, and 3800 G. Such spectra are usually associated with well-isolated triplet spin states with relatively small zero-field splitting. When the systems are cooled to 110 K, the resolution of spectral line improves considerably as a result of the signal narrowing induced apparently by the increasing spin-lattice relaxation time. At 110 K, the central line began to show an axial signal with partially resolved hyperfine splitting in the low-field region originated by a spin doublet $S=1/2$ interacting with a single $I=3/2$ nucleus. This type of signal is characteristic of an isolated Cu^{II} chromophore with an axial g tensor ($g_{\parallel}=2.21$ and $g_{\perp}=2.09$).[34]

The EPR results of **4** show that the Co^{2+} ions are in the high-spin state with three unpaired electrons. However, the spectroscopic complexities of high-spin Co^{2+} with respect to the orbital degeneracy of the ground state and coupling of excited-state terms with changes in coordination environment permit only a qualitative characterization. To understand the EPR results, consider the term-splitting diagram for high-spin Co^{2+} in crystal fields of different symmetry. The influence of the crystal-field and spin-orbit coupling of the electronic properties of transition-metal ions is discussed in the literature.[35] Splitting of spectroscopic states of high-spin Co^{2+} in coordination complexes results in two general patterns arising from the combined effects of the symmetry of the crystal-field and spin-orbit coupling.[36] They correspond to a high-spin d^7 configuration either in an orbitally nondegenerate ground state ($^4A_2$) or in an orbitally degenerate ground state ($^4T_1$), in which the orbital levels are separated by spin-orbit coupling. At 110 K, the EPR spectra of **4** display a very broad band centered at an average g value of 2.07 with a very weak but distinct hyperfine splitting pattern resulting from the interaction of the unpaired electron with the ^{59}Co nucleus ($I=7/2$), and two narrow symmetric bands centered at average g values of 4.15 and 7.36 that are attributed to the characteristics of high spin Co^{2+}. The very broad absorption band can occur from the ferromagnetic-spin-coupling interactions confirmed by the magnetic susceptibility measurement.[37] However, when the temperature increases to room temperature, the EPR signals centered at an average $g=4.15$ and 7.36 become weak, probably mainly caused by the negative zero-field splitting between the $M_s=\pm 1/2$ and $M_s=\pm 3/2$ Kramers doublets, which is in accordance with the ligand-field energy-level diagram of the ground state $^4A_2$ of high-spin Co^{2+}.[38] As the temperature increases from 110 K to room temperature, the Co^{2+} ions tend to populate $M_s=\pm 3/2$ level, which is not EPR-active, so that the EPR signals are almost undetectable at room temperature.

Magnetic Properties

The solid-state magnetic behaviors of **1–4** have been investigated in the temperature range 1.8–300.0 K. The temperature dependence of the magnetic susceptibility of **1** is shown

in Figure 12 in the form of a $\chi_M T$ and a χ_M versus T plot. The measured $\chi_M T$ value of 10.20 emu K mol^{-1} at room temperature, is slightly lower than that expected for 2.5 $S=5/2$

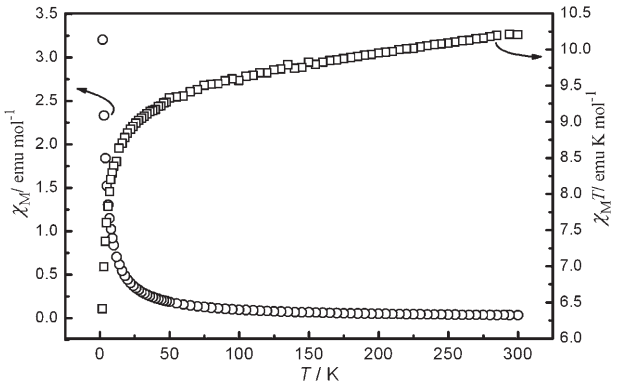

Figure 12. Plots of the temperature dependence of χ_M, $\chi_M T$ for **1**, recorded on a powder sample at an applied field of 0.1 T.

uncorrelated spins (10.94 emu K mol^{-1}). As the temperature is lowered, $\chi_M T$ value decreases steadily to a minimum value of 6.41 emu K mol^{-1} at 1.8 K, indicating the presence of weak antiferromagnetic coupling. The magnetic susceptibility follows the Curie–Weiss law over the entire temperature range with $C=1.02$ emu K mol^{-1} and $\theta=-0.42$ K (Figure S7 in the Supporting Information). This behavior indicates the presence of the weak antiferromagnetic exchange interactions between the Mn^{II} ions.

Figure 13 shows the experimental data of **2** plotted as the $\chi_M T$ versus T and χ_M versus T. The effective moment $\chi_M T$ value of 12.51 emu K mol^{-1} at 300 K is in approximate agreement with the spin-only value of 13.13 emu K mol^{-1} for three noninteracting Mn^{II} ions ($g=2$, $S=5/2$). Subsequently, the effective moment $\chi_M T$ decreases continuously with decreasing temperature. Below 34 K, $\chi_M T$ quickly decreases and then reaches a minimum value of 4.82 emu K mol^{-1} at 1.8 K. This behavior indicates the presence of relatively strong antiferromagnetic interactions between the Mn^{II} ions.

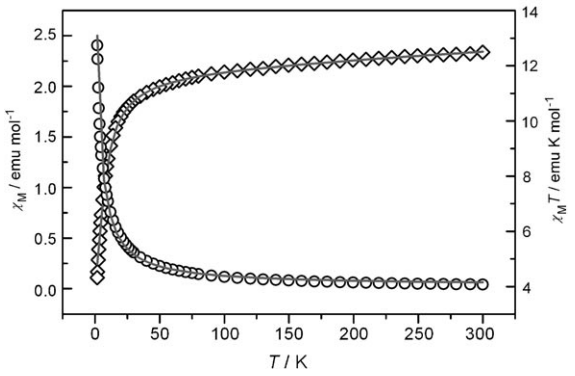

Figure 13. Plots of the temperature dependence of χ_M, $\chi_M T$ for **2**, recorded on a powder sample at an applied field of 0.2 T. Solid line corresponds to the best fit (see text).

As seen from the structures (Figures 2a and b), to obtain an operative expression for the magnetic susceptibility that allows us to evaluate the strength of the exchange interactions, some approximations are needed to decrease the large number of adjustable parameters. Compound **2** can be considered as a uniform chain formed by Mn–(μ-OAc)–Mn dinuclear units, rejecting the Mn···Mn exchange interaction through the Mn–O–Na–O–Mn links. The analytical expression for the dimer model can be applied, which is derived from the exchange Hamiltonian in Equation (2):

$$H = -2\Sigma_{nn} \boldsymbol{J S_i} \cdot \boldsymbol{S_j} \tag{2}$$

Because the acetate bridge leads to the long Mn···Mn separation of 6.177 Å, it is believed that the magnetic exchange interaction between the neighboring two Mn^{II} ions is weak with the exchange integral J. The corresponding energy eigenvalue $E(S_T)$ from Equation (2) is given in Equation (3):

$$E(S_T,S_1,S_2) = E(S_T,S) = -J[S_T(S_T+1)-2S(S+1)] \tag{3}$$

The following Equation (4) was used for calculating the molar magnetic susceptibility of the μ-acetato dimanganese(II) system in compound **2**.

$$\chi_{dimer} = \frac{Ng^2\beta^2}{3kT} \times \frac{\sum_S S_T(S_T+1)(2S_T+1)e^{-E(S_T)/kT}}{\sum_S (2S_T+1)e^{-E(S_T)/kT}} \tag{4}$$

So the expression of χ_{dimer} for **2** is given by Equation (5):

$$\chi_{dimer} = \frac{2g^2\beta^2}{kT} \frac{\{e^{(2J/kT)} + 5e^{(6J/kT)} + 14e^{(12J/kT)} + 30e^{(20J/kT)} + 55e^{(30J/kT)}\}}{\{1 + 3e^{(2J/kT)} + 5e^{(6J/kT)} + 7e^{(12J/kT)} + 9e^{(20J/kT)} + 11e^{(30J/kT)}\}} \tag{5}$$

where N is the Avogadro number, g is the Landé factor, k is the Boltzmann constant, β is the electron Bohr magneton, and T is the temperature in Kelvin. Considering the molar magnetic susceptibility contribution $\chi_{iso}=(Ng^2\beta^2/3kT)S(S+1)$ of an isolated paramagnetic Mn^{2+} ion, the total susceptibilities of trinuclear Mn^{II} species are presented as Equation (6):

$$\chi_M = \chi_{dimer} + \chi_{iso} = 0.75g^2 \frac{\{e^{(x)} + 5e^{(3x)} + 14e^{(6x)} + 30e^{10(x)} + 55e^{(15x)}\}}{\{1 + 3e^{(x)} + 5e^{(3x)} + 7e^{(6x)} + 9e^{(10x)} + 11e^{(15x)}\}} + \frac{1.09375g^2}{T} \tag{6}$$

with $x=2J/k\ T$

The experimental data were fitted using Equation (6), and the value of the exchange interactions were determined as $J=-0.552$ cm^{-1}, and $g=1.901$. This is in good agreement with $g=2.00$, the expected value for a ^6A ground state Mn^{II} and weak coupling mediated by a bridging carboxylate ligand, which is comparable to those previously reported for

carboxylate-bridged manganese(II) complexes with similar bridging networks.[39]

As for compound **3**, the variable-temperature magnetic susceptibility data at 2 K was plotted in Figure 14. Figure 14 shows the $\chi_M T$ value to be about 1.56 emu mol^{-1} K at room

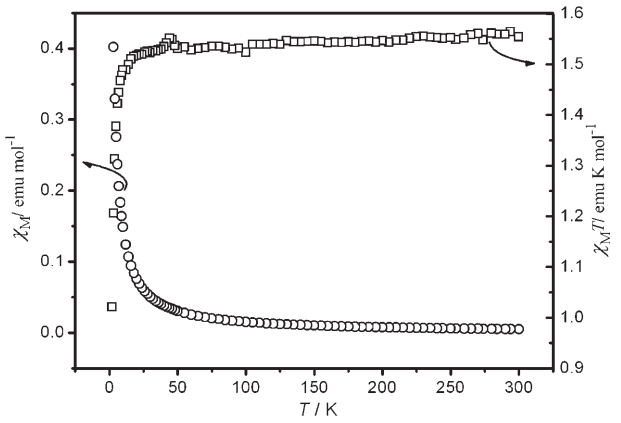

Figure 14. Plots of the temperature dependence of χ_M, $\chi_M T$ for **3**, recorded on a powder sample at an applied field of 0.1 T.

temperature, close to that expected for four noninteracting $S=1/2$ spins (1.50 emu K mol^{-1}). The $\chi_M T$ value decreases slowly with decreasing temperature, reaching a minimum of 1.53 emu K mol^{-1} at 50 K, then subsequently increases sharply to a maximum of 1.55 emu K mol^{-1} at 44 K and then falls to the final minimum value 1.02 emu K mol^{-1} at 1.8 K. The data clearly implies that antiferromagnetic exchange interactions occurr between the four Cu^{II} ions with the spin-canting phenomenon. The magnetic data obey the Curie–Weiss law over the entire temperature range, the fitting gives values of $C=1.56$ emu K mol^{-1} and $\theta=-0.37$ K (see Figure S8 in the Supporting Information), characteristic of an overall weak antiferromagnetic interaction.

The thermal dependence ($\chi_M T$) of **4** is shown in Figure 15. The $\chi_M T$ value at 300 K is 8.82 emu K mol^{-1}, which is much higher than the spin-only value of 5.63 emu K mol^{-1} for

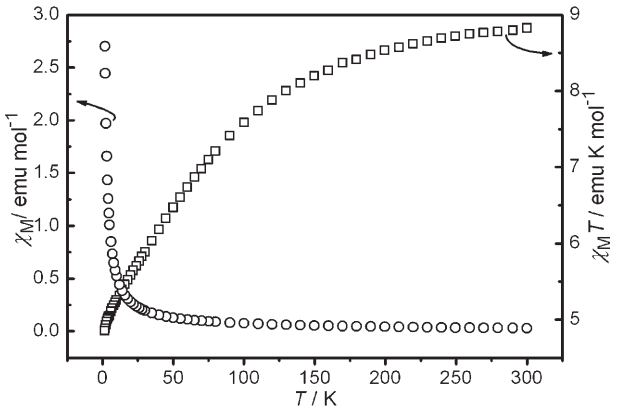

Figure 15. Plots of the temperature dependence of χ_M, $\chi_M T$ for **4**, recorded on a powder sample at an applied field of 0.2 T.

three isolated Co^{II} ions, which further indicates an appreciable spin-orbit coupling expected for the Co^{II} ions.[40] As the temperature is lowered, the $\chi_M T$ value decreases continuously to a minimum value of 4.85 emu K mol^{-1} at 1.8 K. The decreasing region of $\chi_M T$ indicates the presence of antiferromagnetic coupling interactions between the Co^{II} ions. In the temperature range of 80–300 K, the susceptibility data are well-described by the Currie–Weiss expression with $C=$ 9.63 emu K mol^{-1} and $\theta=-26.43$ K (see Figure S9 in the Supporting Information). This behavior indicates antiferromagnetic exchange interactions between the Co^{II} ions.

Conclusions

Five sandwich type transition-metal-substituted tungstoantimonate have been synthesized by the rational method. Compounds **2**, **3**, and **5** display intriguing extended structures. Compound **2** is the first example of a one-dimensional sinusoidal chain based on sandwich type tungstoantimonate by means of the organic acetate bridging ligand. Compound **3** indicates the 2D-netlike structure firstly observed in the antimony-containing sandwich POMs chemistry. Notice that polyoxoanion **5a** maintains a sandwich type structure resulting from the fusion of two $[B\text{-}\beta\text{-}SbW_9O_{33}]^{9-}$ fragments by the three cobalt and one tungsten atoms, further constructing a 3D-netlike structure by the connectivity of Co^{2+} and Na^+ ions. **1** and **2** were simultaneously accomplished from the same system, showing that the lacunary polyoxoanion precursor is not necessary for the preparation of TMSPs. Successful syntheses of **3**–**5** reveal that the $[NaSb_9W_{21}O_{86}]^{18-}$ precursor is metastable in a warm solution and tends to isomerise to $[B\text{-}SbW_9O_{33}]^{9-}$ fragments. The new strategy of design and assembly depicted in this paper may be a promising technique for the construction of many other extended structures with sandwich type metal-oxo clusters, which will open a new avenue in the exploration of sandwich type polyoxometalates. EPR studies for **2**, **3**, and **4** at 110 K and room temperature reveal that the square-pyramidal geometry of metal cations (Mn^{2+}, Cu^{2+}, Co^{2+}) reside in the core of sandwich like complexes. Magnetic behaviors of **1**–**4** display the presence of weak antiferro-magnetic coupling interactions between magnetic metal centers.

Experimental Section

Materials and Methods

All reagents were used as purchased without further purification. The $(NH_4)_{18}[NaSb_9W_{21}O_{86}]\cdot 24H_2O$ precursor was synthesized as described in ref. [27] Variable-temperature magnetic susceptibility data on polycrystalline samples with acceptable purity of compounds **1**–**4** were obtained on a SQUID magnetometer (Quantum Design, MPMS-7) in the temperature region of 1.8–300 K with an applied field of 0.2 or 0.1 T. EPR experiments of compounds **2**, **3** and **4** were performed on a BrukerER-2000-DSRC10 spectrometer at the X-band at 300 and 110 K. IR spectra were recorded in the range of 400–4000 cm^{-1} on an Alpha Centaurt FTIR spectrophotometer by using KBr pellets. Elemental analyses (C and H) were performed on a Perkin–Elmer 2400-CHN elemental analyzer. In-

Table 1. Crystallographic data structure refinement for compounds **1**-**5**.

Compound	**1**	**2**	**3**	**4**	**5**
Empirical formula	$H_{82}Mn_{2.5}Na_2Sb_2W_{19.5}O_{106}$	$C_4H_{72}Mn_3Na_7Sb_2W_{18}O_{96}$	$H_{50}Cu_4Na_3Sb_2W_{18}ClO_{87}$	$H_{30}Co_3K_2Na_{10}Sb_2W_{18}O_{81}$	$H_{40}Co_3Na_5O_{85.5}Sb_2W_{19}$
M_r [g mol^{-1}]	5790.56	5535.17	5353.78	5363.93	5436.71
Crystal system	monoclinic	orthorhombic	orthorhombic	orthorhombic	Triclinic
Space group	$P2_1/n$	*Pbcm*	$P42m$	*Pnma*	$P\bar{1}$
a [Å]	12.9058(2)	15.2820(3)	16.834(2)	30.579(10)	12.0974(14)
b [Å]	25.2780(4)	21.2003(4)	16.834(2)	15.073(5)	17.869(2)
c [Å]	16.1759(3)	30.4213(5)	13.729(3)	19.180(6)	20.323(2)
α [°]	90	90	90	90	92.6870(10)
β [°]	94.144(10)	90	90	90	91.444(2)
γ [°]	90	90	90	90	107.111(2)
V [Å^3]	5263.31(15)	9856.0(3)	3890.5(11)	8840(5)	4190.6(8)
ρ_{cald} [g cm^{-3}]	3.654	3.730	4.570	4.030	4.309
Z	2	4	2	4	2
$\mu(Mo_{K\alpha})$ [mm^{-1}]	22.124	21.961	28.410	24.704	27.302
T [K]	273(2)	273(2)	273(2)	273(2)	273(2)
Reflns measured	47710	109928	12630	40011	19416
Independent reflns	9250	8803	3492	7726	13517
Observed reflns	5119	9800	4692	9364	4738
Parameters	704	682	288	559	1108
R_1 [$I>2\sigma(I)$]	0.0381	0.0377	0.0454	0.0536	0.0592
wR_2 (all data)	0.0895	0.1032	0.1032	0.1267	0.1442

ductively coupled-plasma (ICP) analysis was performed on a Jarrel-Ash J-A1100 spectrometer. Room-temperature XPS experiments were conducted using a Kratos Axis Ultra spectrometer with monochromatized Al Kα radiation (1486.6 eV). The spectrometer was calibrated by using the binding energy of the C 1 *s* line (284.8 eV).

Syntheses

1 and 2: $MnSO_4{\cdot}H_2O$ (0.33 g, 1.96 mmol), Sb_2O_3 (0.13 g, 0.444 mmol) and $Na_2WO_4{\cdot}2H_2O$ (2.64 g, 8.0 mmol) were successively dissolved in sodium acetate buffer (40 mL, 0.5 M, pH 5.0) with stirring. The mixture was heated at 80 °C for two hours with constant stirring, then cooled to room temperature, and filtered. Slow evaporation of the clear filtrate afforded two different single crystals, $H_{82}Mn_{2.5}Na_2Sb_2W_{19.5}O_{106}$ (**1**, 0.86 g, 36% based on $Na_2WO_4{\cdot}2H_2O$) and $C_4H_{72}Mn_3Na_7Sb_2W_{18}O_{96}$ (**2**, 1.06 g, 43% based on $Na_2WO_4{\cdot}2H_2O$), that were suitable for X-ray diffraction. IR (KBr) of **1**: $\tilde{\nu}$ = 943 (s), 837 (vs), 769 (s), 710 (m), 669 (s), 493 (w), 469 cm^{-1} (w); **2**: $\tilde{\nu}$ = 1559 (s), 938 (s), 865 (vs), 779 (s), 729 (vs), 503 (w), 459 (m), 436 cm^{-1} (w); elemental analysis calcd (%) for **1**: Mn 2.37, Na 0.79, Sb 4.21, W 61.91; found: Mn 2.46, Na 0.84, Sb 4.28, W 61.64. Calcd (%) for **2**: C 0.87, H 1.30, Mn 2.98, Na 2.91, Sb 4.40, W 59.79; found: C 0.83, H 1.34, Mn 3.04, Na 2.97, Sb 4.54, W 59.34.

3: The precursor $(NH_4)_{18}[NaSb_9W_{21}O_{86}]{\cdot}24H_2O$ (2.13 g, 0.3 mmol) was first dissolved in distilled water (30 mL), to which $CuCl_2{\cdot}2H_2O$ (0.16 g, 1.0 mmol) was added gradually with stirring. Then the mixture was heated in a 80 °C water bath for one hour, and subsequently cooled to ambient temperature, filtered, and left to evaporate at room temperature. $H_{50}Cu_4Na_3Sb_2W_{18}ClO_{87}$ (**3**, 1.05 g, 56% based on $(NH_4)_{18}[NaSb_9W_{21}O_{86}]{\cdot}24H_2O$) was afforded as green polyhedral crystals several days later. IR (KBr): $\tilde{\nu}$ = 943 (s), 892 (s), 840 (m), 728 (vs), 671 (m), 569 (w), 513 cm^{-1} (m); elemental analysis calcd (%) for **3**: Cu 4.75, Na 1.29, Sb 4.55, W 61.81; found: Cu 4.74, Na 1.34, Sb 4.51, W 61.54.

4 and 5: The precursor $(NH_4)_{18}[NaSb_9W_{21}O_{86}]{\cdot}24H_2O$ (1.07 g, 0.15 mmol) was first dissolved in distilled water (15 mL), to which the solid $CoCl_2{\cdot}6H_2O$ (0.27 g, 1.0 mmol) was added gradually with stirring, thereafter a solution of KOH (10 mL, 0.2 M) was added in drips. The mixture was heated at 80 °C for two hours, then cooled to room temperature, filtered, and left to evaporate slowly at ambient temperature. $H_{30}Co_3K_2Na_{10}Sb_2W_{18}O_{81}$ (**4,** 0.57 g, 61% based on $Na_2WO_4{\cdot}2H_2O$) and $H_{40}Co_3Na_5O_{85.5}Sb_2W_{19}$ (**5,** 0.21 g, 23% based on $Na_2WO_4{\cdot}2H_2O$) were afforded as greenish black and deep red crystals, respectively. Both types of crystals were obtained simultaneously after several weeks, and were manually separated and purified. Elemental analysis calcd (%) for **4**: Co 3.30, K 1.46, Na 4.29, Sb 4.54, W 61.69; found: Co 3.25, K 1.44, Na 4.34, Sb 4.46, W 61.24. Calcd (%) for **5**: Co 3.25, Na 2.11, Sb 4.48, W 64.25; found: Co 3.31, Na 2.14, Sb 4.53, W 63.88.

X-ray Crystallographic Studies of the Compounds

Intensity data were collected on a RigaKu RAXIS-IV diffractometer with graphite-monochromated $Mo_{K\alpha}$ (λ = 0.71073 Å) radiation at room temperature. The structures were solved by direct methods and refined using full-matrix least squares on F^2. All calculations were performed using the *SHELXL*-97 program package.[28] Empirical absorption correction was applied. All of the non-hydrogen atoms were refined anisotropically. The organic hydrogen atoms were generated geometrically, however the aqua hydrogen atoms were not located. A summary of crystal data and structure refinement for compounds **1**–**5** is listed in Table 1. CCDC 623893 (**2**) contains the supplementary crystallographic data for this paper. These data can be obtained free of charge from The Cambridge Crystallographic Data Centre by using www.ccdc.cam.ac.uk/data_request/cif. Further details of the crystal structure investigations may be obtained from the Fachinformationszentrum Karlsruhe, 76344 Eggenstein-Leopoldshafen, Germany (fax: (+49) 7247-808-666; e-mail: crystal@fiz-karlstruhe.de) and quoting the deposition numbers CSD 417113 (**1**), 417114 (**3**), 417115 (**4**), 417116 (**5**).

Acknowledgements

The authors thank the Natural Science Foundation of China, the Program for New Century Excellent Talents in University of Henan Province, the Foundation of Education Department of Henan Province, and the Natural Science Foundation of Henan Province for financial support.

[1] a) *Polyoxometalate Chemistry: From Topology via Self-Assembly to Applications* (Eds: M. T. Pope, A. Müller), Kluwer, Dordrecht, **2001**; b) R. Thouvenot, M. Michelon, A. Tézé, G. Hervé in *Polyoxometalate: From Platonic Solids to Anti-Retroviral Activity* (Eds: M. T. Pope, A. Müller), Kluwer, Dordrecht, **1994**, pp. 177–190.; c) N. Mizuno, M. Misono, *Chem. Rev.* **1998**, *98*, 199–217.

[2] a) M. T. Pope in *Heteropoly and Isopoly Oxometalates*, Springer, Berlin, **1983**; b) M. T. Pope, A. Müller, *Angew. Chem.* **1991**, *103*, 56–70; *Angew. Chem. Int. Ed. Engl.* **1991**, *30*, 34–38; c) A. Müller,

F. Peters, M. T. Pope, D. Gatteschi, *Chem. Rev.* **1998**, *98*, 239–271; d) A. Müller, S. Roy, *Coord. Chem. Rev.* **2003**, *245*, 153–166.

[3] a) A. Müller, E. Krickemeyer, H. Bögge, M. Schmidtmann, C. Beugholt, P. Kögerler, C. Lu, *Angew. Chem.* **1998**, *110*, 1278–1281; *Angew. Chem. Int. Ed.* **1998**, *37*, 1220–1223; b) A. Müller, S. Q. N. Shah, H. H. Bögge, M. Schmidtmann, *Nature* **1999**, *397*, 48–50; c) K. Wassermann, M. H. Dickman, M. T. Pope, *Angew. Chem.* **1997**, *109*, 1513–1516; *Angew. Chem. Int. Ed. Engl* **1997**, *36*, 1445–1448; d) A. Müller, P. Kögerler, C. Kuhlmann, *Chem. Commun.* **1999**, 1347–1358; e) A. Müller, C. Serain, *Acc. Chem. Res.* **2000**, *33*, 2–10; f) J. Niu, P. Ma, H. Niu, J. Li, J. Zhao, Y. Song, J. Wang, *Chem. Eur. J.* **2007**, *13*, 8739–8748; g) V. Soghomonian, Q. Chen, R. C. Haushalter, J. Zubieta, *Angew. Chem.* **1993**, *105*, 601–603; *Angew. Chem. Int. Ed. Engl.* **1993**, *32*, 610–612; h) M. I. Khan, L. M. Meger, R. C. Haushalter, A. L. Schweitzer, J. Zubieta, J. L. Dye, *Chem. Mater.* **1996**, *8*, 43–53.

[4] C. D. Wu, C. Z. Lu, H. H. Zhuang, J. S. Huang, *J. Am. Chem. Soc.* **2002**, *124*, 3836–3837.

[5] A. Müller, E. Beckmann, H. Bögge, M. Schmidtmann, A. Dress, *Angew. Chem.* **2002**, *114*, 1210–1215; *Angew. Chem. Int. Ed.* **2002**, *41*, 1162–1167.

[6] M. T. Pope in *Polyoxo Anions: Synthesis and Structure. In Comprehensive Coordination Chemistry II*: *Transition Metal Groups 3–6*, *Vol. 4* (Ed.: A. G. Wedd), Elsevier, New York, **2004**, pp. 635–678.

[7] a) M. T. Pope, *Comp. Coord. Chem. II* **2003**, *4*, 635–678; b) S.-T. Zheng, M.-H. Wang, G. -Y, Yang, *Chem. Asian J.* **2007**, *2*, 1380–1387.

[8] a) T. J. R. Weakly, H. T. Evans, J. S. Showell, G. F. Tourné, C. M. Tourné, *J. Chem. Soc. Chem. Commun.* **1973**, 139–140; b) T. J. R. Weakley, R. G. Finke, *Inorg. Chem.* **1990**, *29*, 1235–1241; c) L. H. Bi, E. B. Wang, J. Peng, R. D. Huang, L. Xu, C. W. Hu, *Inorg. Chem.* **2000**, *39*, 671–679; d) U. Kortz, S. Isber, M. H. Dickman, D. Ravot, *Inorg. Chem.* **2000**, *39*, 2915–2922.

[9] a) F. Robert, M. Leyrie, G. Hervé, *Acta Crystallogr. Sect. B* **1982**, *38*, 358–362; b) M. Bösing, A. Nöh, I. Loose, B. Krebs, *J. Am. Chem. Soc.* **1998**, *120*, 7252–7259; c) B. Botar, T. Yamase, E. Ishikawa, *Inorg. Chem. Commun.* **2001**, *4*, 551–554.

[10] a) E. M. Limanski, D. Drewes, E. Droste, R. Bohner, B. Krebs, *J. Mol. Struct.* **2003**, *656*, 17–25; b) D. Drewes, E. M. Limanski, M. Piepnbrink, B. Krebs, *Z. Anorg. Allg. Chem.* **2004**, *630*, 58–62.

[11] a) W. H. Knoth, P. J. Domaille, R. D. Farlee, *Organometallics* **1985**, *4*, 62–68; b) F. B. Xin, M. T. Pope, *J. Am. Chem. Soc.* **1996**, *118*, 7731–7736; c) R. G. Finke, B. Rapko, T. J. R. Weakley, *Inorg. Chem.* **1989**, *28*, 1573–1579.

[12] a) E. Cadot, M. A. Pilette, J. Marrot, F. Sécheresse, *Angew. Chem.* **2003**, *115*, 2223–2226; *Angew. Chem. Int. Ed.* **2003**, *42*, 2173–2176; b) S. S. Mal, U. Kortz, *Angew. Chem.* **2005**, *117*, 3843–3846; *Angew. Chem. Int. Ed.* **2005**, *44*, 3777–3780; c) P. Mialane, A. Dolbecq, J. Marrot, E. Rivière, F. Sécheresse, *Angew. Chem.* **2003**, *115*, 3647–3650; *Angew. Chem. Int. Ed.* **2003**, *42*, 3523–3526.

[13] *Polyoxometalate Chemistry for Nano-Composite Design* (Eds: T. Yamase, M. T. Pope), Kluwer, Dordrecht, **2002**.

[14] *Polyoxometalate Molecular Science* (Eds.: J. J. Borrás-Almeanar, E. Coronado, A. Müller, M. T. Pope), Kluwer, Dordrecht, **2003**.

[15] A. Müller, M. T. Pope, A. Merca, H. Bögge, M. Schmidtmann, J. V. Slageren, M. Dressel, D. G. Kurth, *Chem. Eur. J.* **2005**, *11*, 5849–5854.

[16] T. Yamase, B. Botar, E. Ishikawa, K. Fukaya, *Chem. Lett.* **2001**, 56–57.

[17] J. Fischer, L. Richard, R. Weiss, *J. Am. Chem. Soc.* **1976**, *98*, 3050–3052.

[18] L. H. Bi, E. B. Wang, R. D. Huang, C. W. Hu, *J. Mol. Struct.* **2000**, *553*, 167–174.

[19] a) H. Naruke, T. Yamase, *J. Alloys Compd.* **1998**, *268*, 100–106; b) H. Naruke, T. Yamase, Y. Sasaki, *J. Chem. Soc. Dalton Trans.* **1990**, 1687–1696.

[20] a) H. Naruke, T. Yamase, *Bull. Chem. Soc. Jpn.* **2001**, *74*, 1289–1294; b) H. Naruke, T. Yamase, *Bull. Chem. Soc. Jpn.* **2002**, *75*, 1275–1282.

[21] T. Yamase, E. Lshikawa, K. Fukaya, H. Nojiri, T. Taniguchi, T. Atake, *Inorg. Chem.* **2004**, *43*, 8150–8157.

[22] a) M. Bösing, I. Loose, H. Pohlmann, B. Krebs, *Chem. Eur. J.* **1997**, *3*, 1232–1237; b) M. Bösing, A. Nöh, I. Loose, B. Krebs, *J. Am. Chem. Soc.* **1998**, *120*, 7252–7259; c) D. Volkmer, B. Bredenkötter, J. Tellenbröker, P. Kögerler, D. G. Kurth, P. Lehmann, H. Schnablegger, D. Schwahn, M. Piepenbrink, B. Krebs, *J. Am. Chem. Soc.* **2002**, *124*, 10489–10496; d) M. Piepenbrink, E. M. Limanskiu, B. Z. Krebs, *Z. Anorg. Allg. Chem.* **2002**, 628, 1187–1191; e) I. Loose, E. Droste, M. Bösing, H. Pohlmann, M. H. Dickman, C. Rosu, M. T. Pope, B. Krebs, *Inorg. Chem.* **1999**, *38*, 2688–2694.

[23] a) U. Kortz, N. K. Al-Kassem, M. G. Savelieff, N. A. Al Kadi, M. Sadakane, *Inorg. Chem.* **2001**, *40*, 4742–4749; b) P. Mialane, J. Marrôt, E. Rivière, J. Nebout, G. Hervé, *Inorg. Chem.* **2001**, *40*, 44–48; c) U. Kortz, M. G. Savelieff, B. S. Bassil, B. Keita, L. Nadjo, *Inorg. Chem.* **2002**, *41*, 783–789; d) L. H. Bi, M. Reicke, U. Kortz, B. Keita, L. Nadjo, R. J. Clark, *Inorg. Chem.* **2004**, *43*, 3915–3920.

[24] F. Hussain, M. Reicke, U. Kortz, *Eur. J. Inorg. Chem.* **2004**, 2733–2738.

[25] D. Laurencin, R. Villanneau, P. Herson, R. Thouvenot, Y. Jeannin, A. Proust, *Chem. Commun.* **2005**, 5524–5526.

[26] T. Yamase, K. Fukaya, H. Nojiri, Y. Ohshima, *Inorg. Chem.* **2006**, *45*, 7698–7704.

[27] G. Hervé, A. Tézé, *Inorg. Synth.* **1990**, *27*, 120–122.

[28] G. M. Sheldrick, SHELXTL 97, University of Göttingen Göttingen (Germany), **1997**.

[29] U. Kortz, S. Nellutla, A. C. Stowe, N. S. Dalal, J. V. Tol, B. S. Bassil, *Inorg. Chem.* **2004**, *43*, 144–154.

[30] N. Laronze, J. Marrot, G. Hervé, *Inorg. Chem.* **2003**, *42*, 5857–5862.

[31] D. J. E. Ingram, *Spectroscopy at Radio and Microwave Frequencies*, *2nd ed.*, Butterworth, London, **1967**.

[32] B. S. Garg, M. R. P. Kurup, S. K. Jain, Y. K. Bhoon, *Transition Met. Chem.* **1988**, *13*, 92–95.

[33] a) J. Owen, E. A. Harris, *Electron Paramagnetic Resonance* (Ed.: S. Geshwind), Plenum, New York, **1972**, pp. 427–492; b) T. Howard, J. Telser, V. J. DeRose, *Inorg. Chem.* **2000**, *39*, 3379–3385; c) S. Blanchard, G. Blondin, E. Rivière, M. Nierlich, J. J. Girerd, *Inorg. Chem.* **2003**, *42*, 4568–4578; d) C. Hureau, S. Blanchard, M. Nierlich, G. Blain, E. Rivière, J. J. Girerd, E. A. Mallart, G. Blondin, *Inorg. Chem.* **2004**, *43*, 4415–4426.

[34] S. Reinoso, P. Vitoria, J. M. Gutierrez-Zorrilla, L. Lezama, L. San Felices, J. I. Beitia, *Inorg. Chem.* **2005**, *44*, 9731–9742.

[35] a) C. J. Ballhausen, *Spin-Orbit Coupling*;,McGraw-Hill, New York, **1962**, chap. VI, p. 113; b) A. Abragam, M. H. L. Pryce, *Proc. R. Soc. London Ser. A* **1951**, *206*, 173; c) J. S. Griffith, *The Theory of Transition-Metal Ions*, Cambridge University Press, London, **1961**, p. 240.

[36] R. L. Carlin, A. J. von Duyneveldt, *Magnetic Properties of Transition Metal Compounds*, Springer, New York, **1977**, chap. 1, p. 1.

[37] T. Hirotsu, A. Sonoda, H. Kanoh, K. Ooi, M. Seno, *J. Phys. Chem. B* **1997**, *101*, 4498–4507.

[38] E. M. El-Malki, D. Werst, P. E. Doan, W. M. H. Sachtler, *J. Phys. Chem. B* **2000**, *104*, 5924–5931.

[39] a) K. F. Hsu, S. L. Wang, *Inorg. Chem.* **2000**, *39*, 1773–1778; b) W. Lin, M. E. Chapman, Z. Wang, G. T. Yee, *Inorg. Chem.* **2000**, *39*, 4169–4173; c) L. Dubois, D.-F. Xiang, X.-S. Tan, J. Pécaut, P. Jones, S. Baudron, L. L. Pape, J.-M. Latour, C. Baffert, S. Chardon-Noblat, M.-N. Collomb, A. Deronzier, *Inorg. Chem.* **2003**, *42*, 750–760; d) S. Durot, C. Policar, G. Pelosi, F. Bisceglie, T. Mallah, J. P. Mahy, *Inorg. Chem.* **2003**, *42*, 8072–8080; e) R. L. F. Rardin, P. Poganiuch, A. Bino, D. P. Goldberg, W. B. Tolman, S. Liu, S. J. Lippard, *J. Am. Chem. Soc.* **1992**, *114*, 5240–5249.

[40] a) R. L. Carlin, *Magnetochemistry*, Springer, New York, **1983**; b) O. Kahn, *Molecular Magnetism*, VCH, Weinheim, **1993**; c) B. Bassil, S. Nellutla, U. Kortz, A. C. Stowe, J. van Tol, N. S. Dalal, B. Keita, L. Nadjo, *Inorg. Chem.* **2005**, *44*, 2659–2665.

Received: October 30, 2007
Revised: February 20, 2008

